doi:10.1038/nature10238

Supplementary Table 1. Data collection and refinement statistics

	Ile217Cys_a[#]	Ile217Cys_b	Met221Cys[$]
Data collection			
Space group	*I*222	*I*222	*I*222
Cell dimensions			
a, *b*, *c* (Å)	125.59, 125.48, 192.30	126.28, 126.14, 192.44	125.50, 125.81, 191.82
α, β, γ (°)	90, 90, 90	90, 90, 90	90, 90, 90
Wavelength (Å)	0.99994	1.005	0.99994
Resolution (Å)	50 – 2.70 (2.76 – 2.70)*	50 – 2.80 (2.87 – 2.80)*	50 – 2.95 (3.02 – 2.95)*
R_{merge}	5.1 (39.4)	5.2 (34.6)	5.1 (63.5)
$I/\sigma I$	23.11 (1.69)	20.61 (2.08)	31.78 (1.52)
Completeness (%)	87.5 (55.6)	89.0 (59.3)	98.5 (85.6)
Redundancy	3.8 (2.9)	3.1 (2.8)	5.6 (3.7)
Refinement			
Resolution (Å)	50 – 2.70	50 – 2.80	50 – 2.95
No. reflections	36,497	31,615	31,353
R_{work}/ R_{free}	26.60/27.30	26.71/29.22	25.89/27.16
No. atoms			
Protein	3621	3595	3653
Ligand/ion	95	132	127
Water	2	2	2
B-factors			
Protein	91.3	94.7	110.5
Ligand/ion	98.1	110.5	123.8
Water	44.6	43.2	50.9
R.m.s deviations			
Bond lengths (Å)	0.0094	0.0092	0.0095
Bond angles (°)	1.189	1.218	1.337

10 mM YCl_3 was added into the cryo solution, but no sign of bound Y^{3+} was evident.
$ This was an SeMet-labeled crystal.
* Highest resolution shells are shown in parentheses.

Supplementary Discussion

Functional state of NavAb

Upon depolarization to 0 mV, the voltage sensors of Na^+ channels activate to generate the pre-open state, the intracellular activation gate opens to allow ion conductance, and the channel then inactivates. The conformation of NavAb in our crystals fits with the expectations for a pre-open state, because the voltage sensors are activated, the selectivity filter is rigid and open, but the pore is closed by the intracellular activation gate. The conformation of NavAb does not fit expectations for the open state because the activation gate is closed at the intracellular end of the pore. The conformation of NavAb also does not fit expectations for the inactivated state. NaChBac and related bacterial sodium channels inactivate by a slow-inactivation mechanism[1], which is thought to involve relaxation and/or collapse of the ion selectivity filter and the pore lining[2-5]. C-type inactivation of K^+ channels is accompanied by a similar rearrangement and partial collapse of the selectivity filter, as observed in recent crystal structures[6]. Because the selectivity filter in our structure is rigidly held open and the lumen of the pore is also open except for the closed activation gate, our structure does not fit the current expectations for an inactivated state.

Conserved selectivity filter architecture in Na_V channels and Ca_V channels

The selectivity filter sequence in the NaChBac channel family is conserved as: TLESW (Fig. 3e and Supplementary Fig. 1). Unlike vertebrate Na_V channels, the selectivity filter in NavAb is contributed by four identical protein subunits. However, conserved sequence hallmarks (Fig. 3e) strongly suggest that the architecture of the Na_V and Ca_V channel pores is highly similar to the pore structure observed in NavAb. In vertebrate Na_V channels, the high field-strength site is formed by the DEKA selectivity motif, but this is EEEE or EEDD in Ca_V channels (Fig. 3e). Therefore, these amino acid differences indicate that NavAb must achieve selectivity for Na^+ over Ca^{2+} through subtly different mechanisms. We anticipate that future structural characterization of Ca^{2+}-selective forms of the NavAb channel (nicknamed CaChBac[7] in Fig. 3e) will help to define the determinants of Na^+ versus Ca^{2+} selectivity.

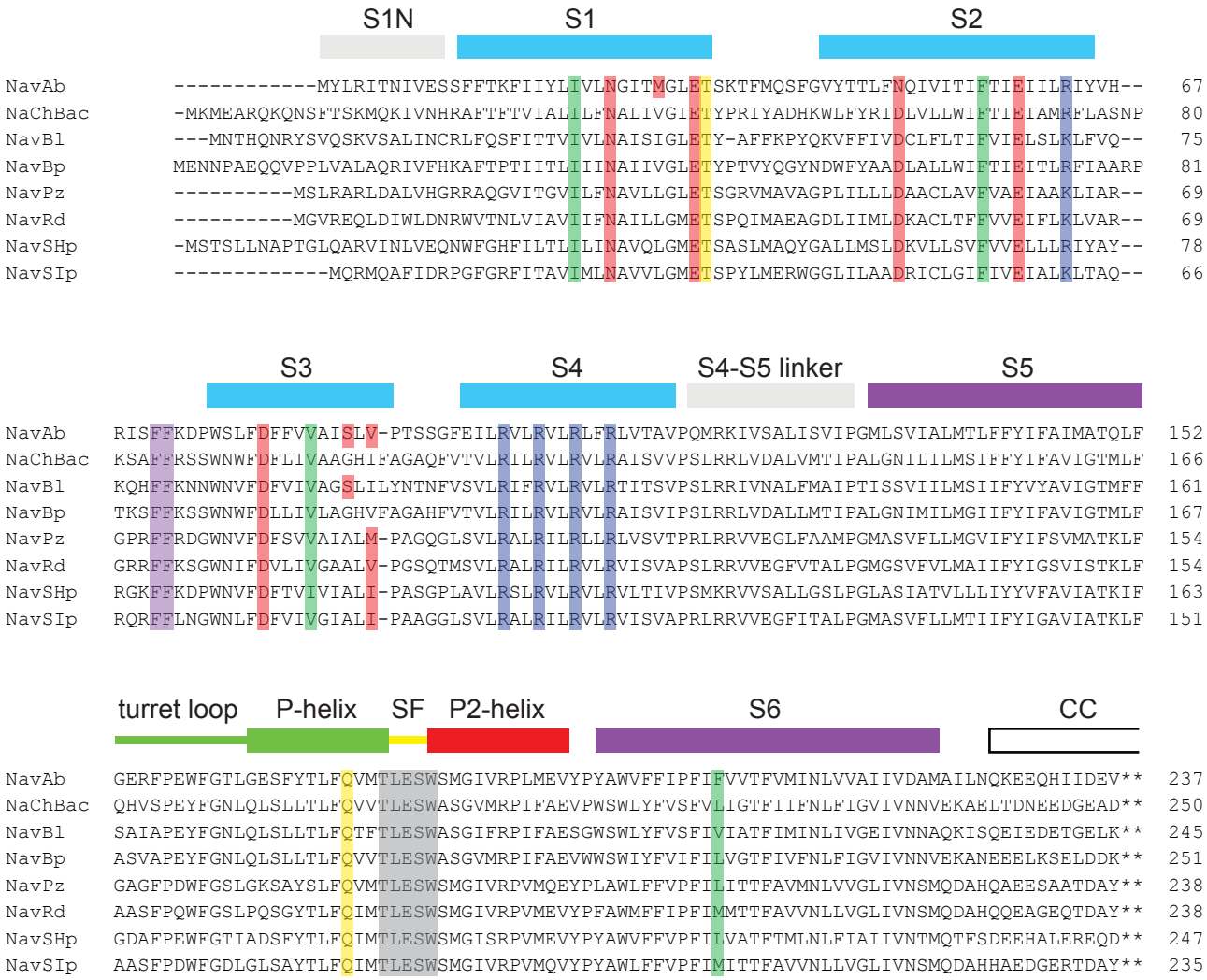

Supplementary Figure 1. Structure-based sequence alignment of NavAb to other bacterial Na$_V$ channels. In addition to NavAb, seven bacterial Na$_V$ channels have been characterized by electrophysiological methods to date[8-11]. These channels are NaChBac (*Bacillus halodurans* C-125), NavBl (*Bacillus licheniformis*), NavBp (*Bacillus pseudofirmus* OF4), NavPz (*Paracoccus zeaxanthinifaciens*), NavRd (*Roseobacter denitrificans*), NavSHp (*Shewanella putrefaciens*) and NavSIp (*Silicibacter pomeroyi* DSS-3). Many residues discussed in the main text are indicated throughout the voltage-sensor domain (S1-S4) and pore module (S5-S6). For example, the intracellular and extracellular negative charge-cluster residues (INC and ENC) and other polar residues are highlighted in orange; the hydrophobic constriction site (HCS) residues and S6 "portal gate" residue are shown in green; and the conserved S1-threonine and P-helix Glu177 interacting residue (Q172 in NavAb) are shown in yellow. For simplicity, only a portion of the ~30-40 amino acids at the intracellular end of the S6 is shown. This region is thought to form a coiled-coil (CC) domain[12,13] and was poorly ordered and therefore not modeled in our structures. However, a portion of this region was visible within the NavAb-Met221Cys density maps (not shown).

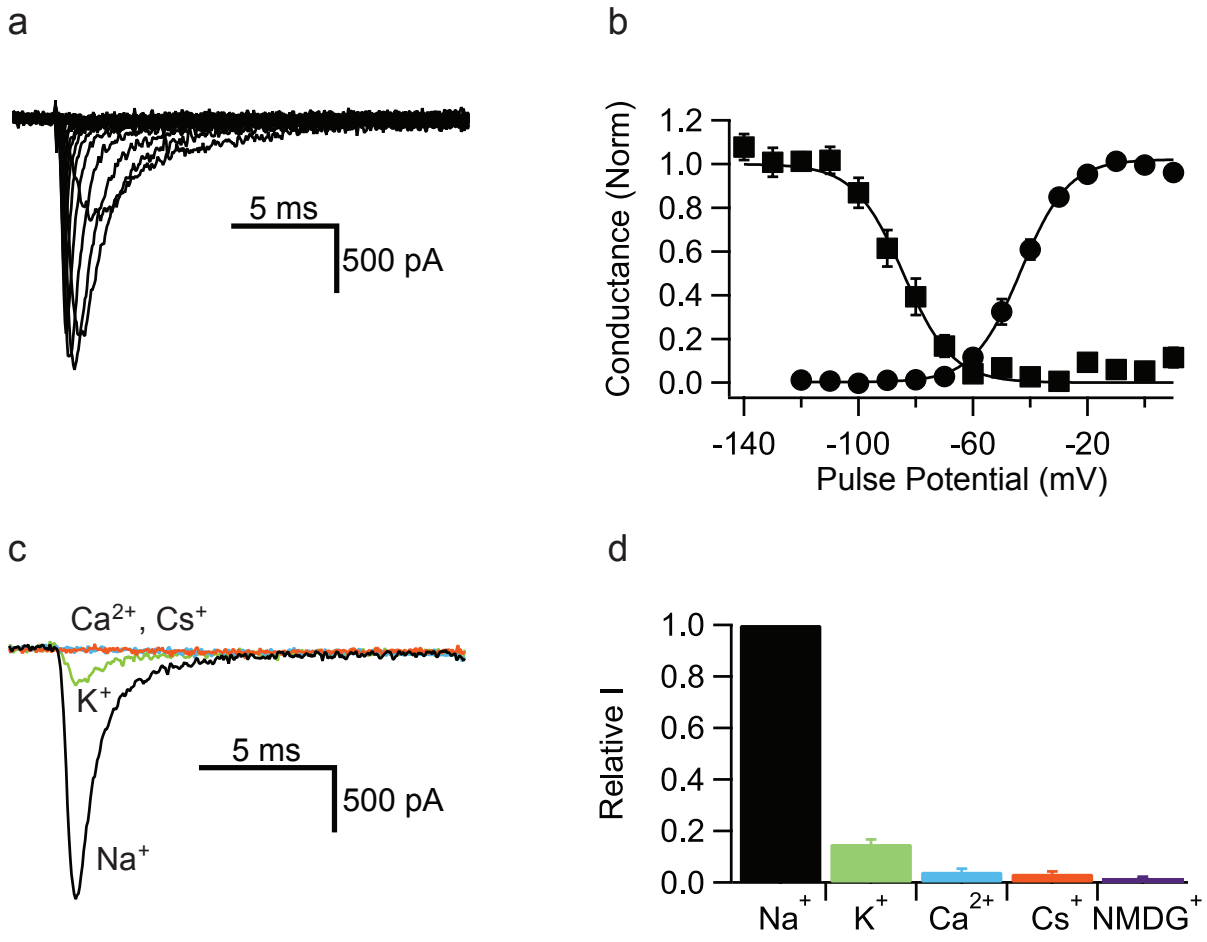

Supplementary Figure 2. Electrophysiological characterization of NavAb. a, Currents measured from NavAb transfected tsA-201 cells elicited by depolarizing pulses ranging from -120 to +90 mV in 10 mV increments. The membrane holding potential was -120 mV. **b,** Mean voltage dependence of activation (circles) and inactivation (squares). To determine mean voltage dependence of activation, peak currents were measured during voltage steps to the indicated potentials and conductance was plotted as $I/(V-V_{rev})$ where V was the test potential and V_{rev}, the apparent reversal potential. Values from individual experiments were normalized to the maximum conductance. Individual normalized conductance voltage curves were fit with a Boltzmann equation, $1/1+\exp[(V_a-V)/k]$ where V_a was the half activation voltage and k was the slope. Mean V_a was -44.1 ± 1.91mV, mean k was 7.5 ± 0.56 mV, n = 9. To determine the voltage-dependence of inactivation, peak currents were measured during test pulses to 20 mV following 500 ms conditioning depolarizations to the indicated potentials. Values from individual cells were normalized to the largest currents following prepulses to strongly negative potentials. Individual normalized inactivation curves were fit with a Boltzmann equation, $1/1+\exp[(V_h-V)/k]$ where V_h was the half inactivation voltage and k was the slope. Mean V_h was -85.6 ± 2.76 mV, mean k was -7.7 ± 1.21mV, n = 5. **c,** Examples of NavAb current traces obtained in a cell exposed sequentially to Na-containing, K-containing, Cs-containing and Ca-containing solutions during depolarizations to 20 mV from a holding potential of -120 mV. **d,** Summary of mean relative NavAb current in cells exposed to solutions containing the indicated ions. Recordings in each test ion-containing solution were flanked by recordings in Na-containing solution; recordings in the test ion-containing solution were normalized to the mean of the flanking recordings in the presence of sodium (n = 7).

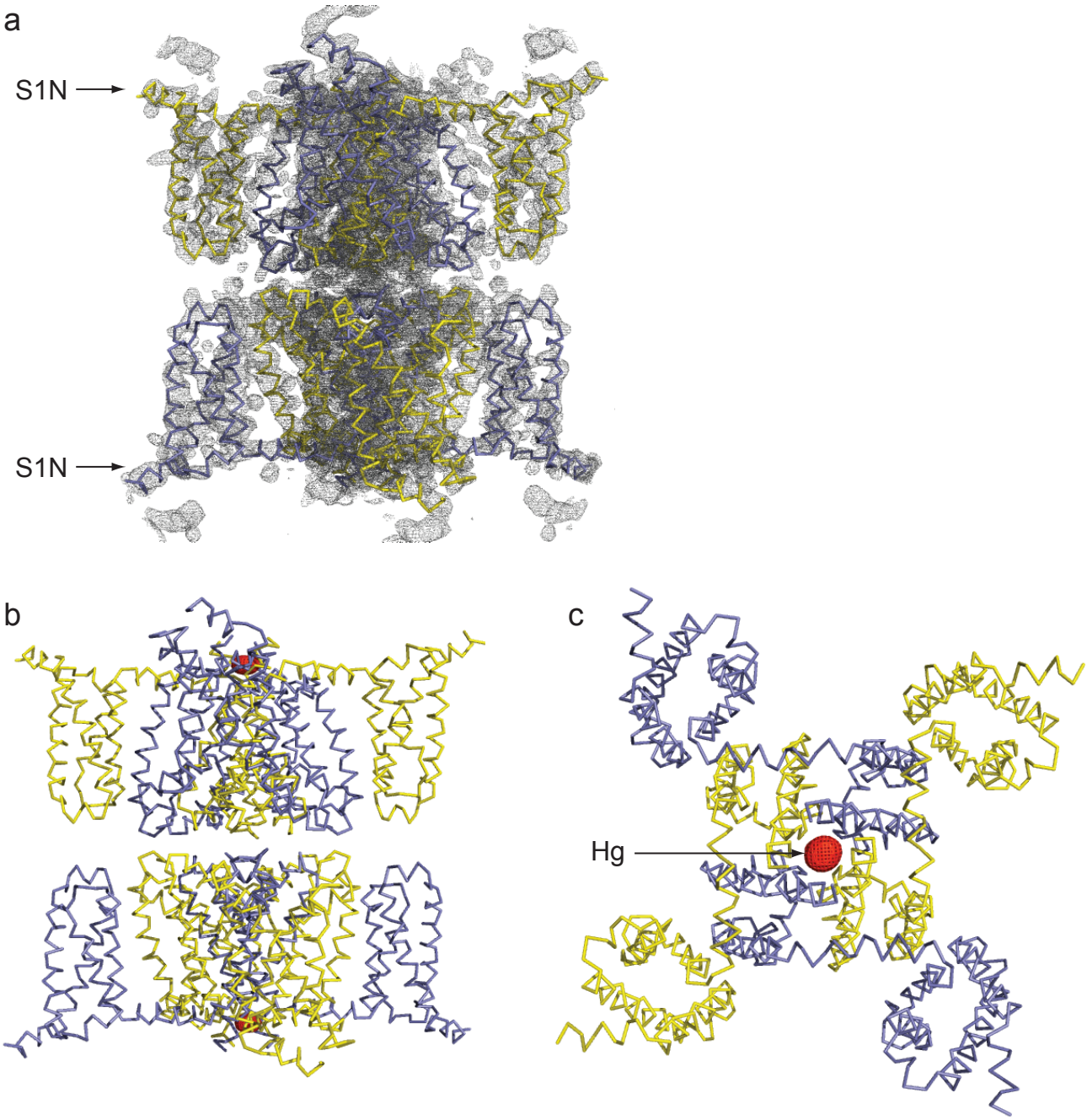

Supplementary Figure 3. Experimentally-phased electron density map of NavAb-Ile217Cys-Hg. **a,** A SAD-data set collected from a NavAb-Ile217Cys crystal complexed with mercury was used in the SOLVE/RESOLVE package[14] as described in Methods. The electron density map calculated from RESOLVE at 3.7 Å is shown here over a portion of the unit cell contoured at 1.5 σ. The final model of NavAb-Ile217Cys refined from a mercury-free 2.7 Å data set helps to illustrate the quality and features of this unbiased experimental map. For example, the relative positions of the S6 pore-lining helices and the S1N helical structure are well defined. Subunits are colored according to their crystallographic symmetry mates (yellow and blue, respectively) so the dimer-of-dimers arrangement within and between channel tetramers can be appreciated. **b,** Same as part **a**, only the map has been contoured at 11 σ and colored red, illustrating the single mercury site within the NavAb tetramer. Because the structural model that is shown here was refined from a native data set without mercury, it is clear that the binding of mercury does not dramatically affect the overall structure of NavAb-Ile217Cys. In this respect, the mercury site further confirms the spatial proximity of the S6 pore-lining helices. **c,** Same as part **b**, viewed from the intracellular side of the membrane.

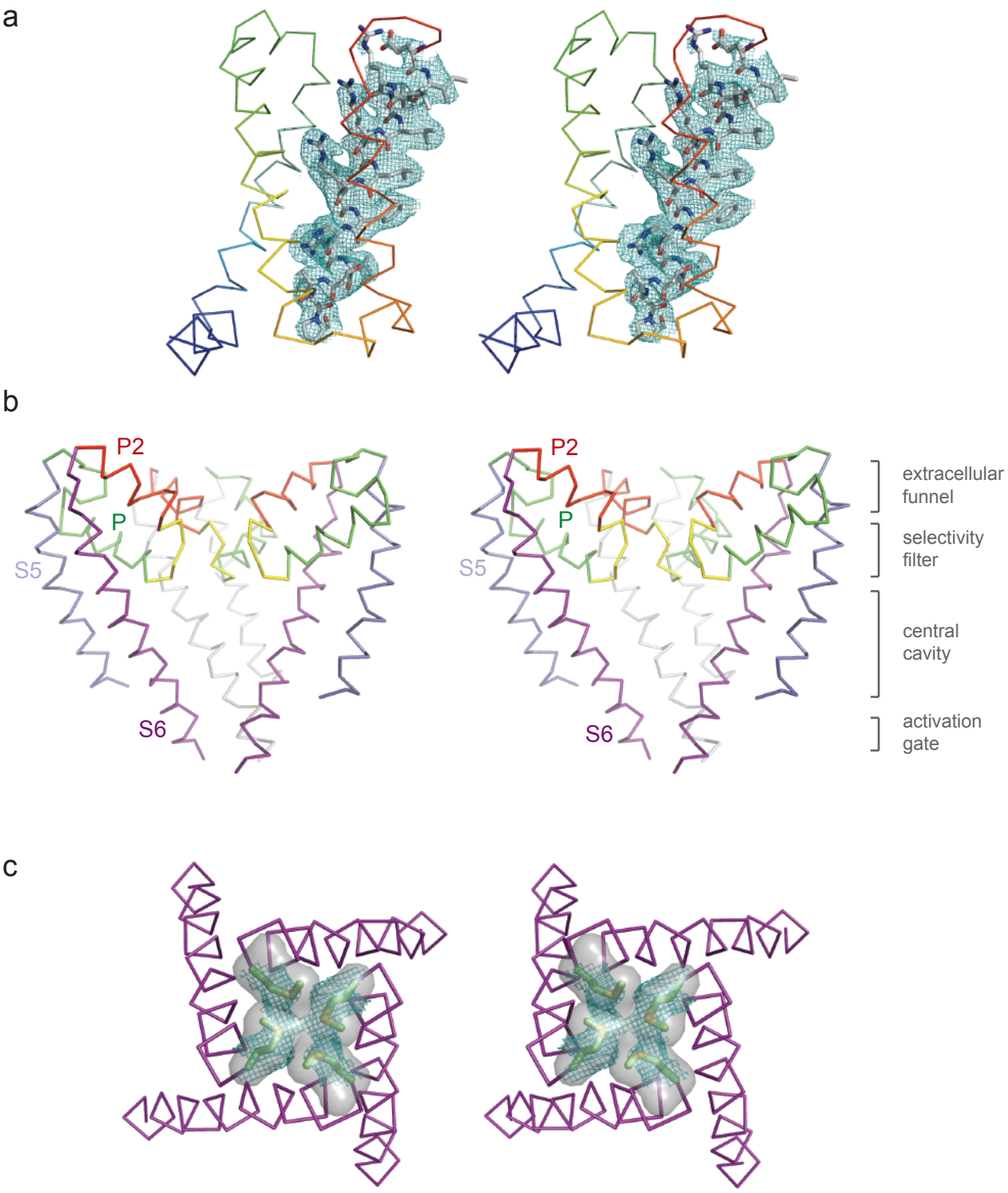

Supplementary Figure 4. Stereo-views of the NavAb VSD and pore module. a, The NavAb-Ile217Cys VSD from the 2.7 Å resolution structure showing residues on the S4 segment in stick representation and a corresponding F_o-F_c omit map of the S4 contoured at 1.5 σ. The rest of the VSD, from S1N to the S4, is shown in ribbon representation and colored from blue to red. **b,** Secondary structural elements of the pore module are colored: S5 (slate), turret loop and P-helix (green), selectivity filter sequence (yellow), P2-helix (red), S6 (purple). The S5 and S6 helices of the distant subunit have been colored grey, and the front subunit has been removed for clarity. **c,** View from the intracellular side of the closed NavAb-Ile217Cys activation gate (2.7 Å resolution structure). Only the S6 helices and the Met221 side-chain are shown for clarity. The electron density is from an F_o-F_c omit map contoured at 1 σ.

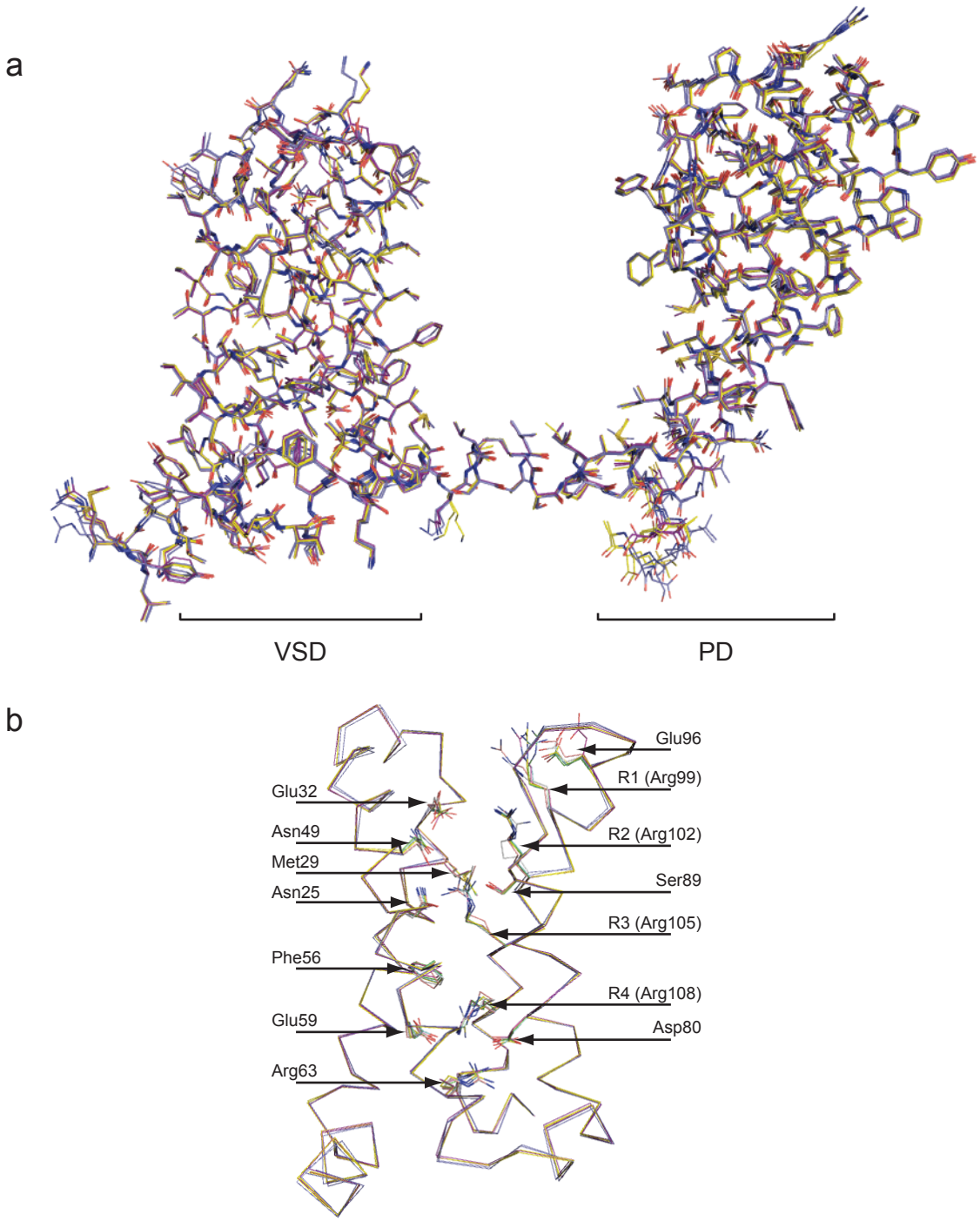

Supplementary Figure 5. Comparison of the NavAb-Ile217Cys and NavAb-Met221Cys crystal structures. a, NavAb crystallized with two molecules in the asymmetric unit, leading to a dimer-of-dimers arrangement. Superposition of all 6 crystallographically independent subunits (i.e. 2 subunits from each NavAb structure) demonstrates their overall similarity; the root mean square deviation is <0.5 Å over all Cα atoms. There are three noteworthy differences: i) All six Met29 side-chains are not found within hydrogen-bonding distance of R3. ii) The closed pore structures differ in their details. Density for Val218-Met221 was not strong enough to reliably model in the 2.8 Å NavAb-Ile217Cys structure. The 2.7 Å NavAb-Ile217Cys pore model is shown in Fig. 2 and Supplementary Fig. 4. The NavAb-Met221Cys (2.95 Å) pore structure is highly similar to the 2.7 Å NavAb-Ile217Cys model, except for a tapering around the Met221Cys side-chains (not shown). iii) The Ser178 side-chain near the selectivity filter is observed in different orientations, as shown in Supplementary Fig. 11. **b,** A superposition of the 6 crystallographically independent NavAb VSDs. Many of the residues highlighted in the main text and Supplementary Fig. 1 are show here as line representations.

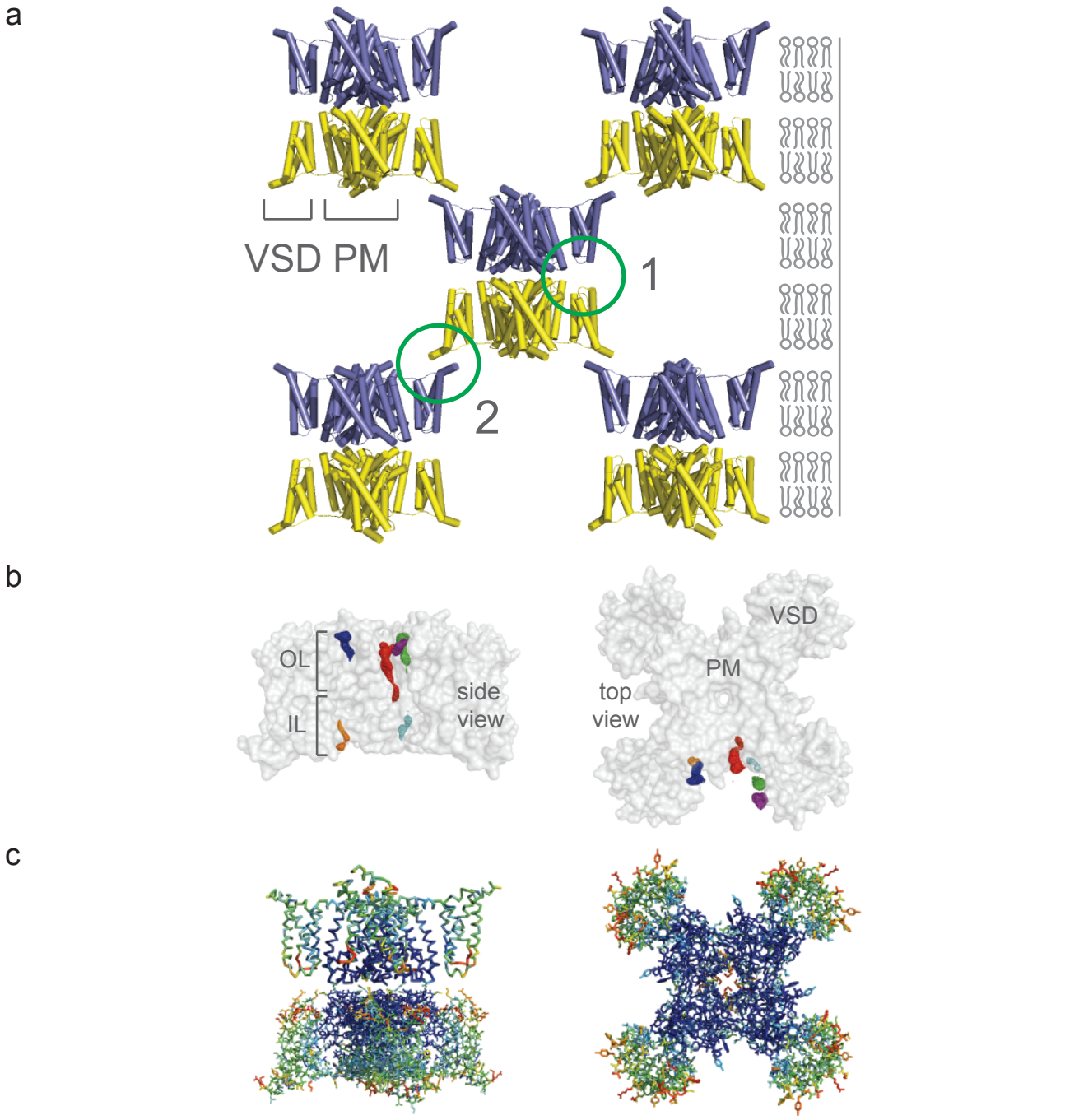

Supplementary Figure 6. Structure of NavAb in a membrane-like environment. a, Crystal packing of NavAb in a membrane-like environment. The stacked layers of NavAb channels observed in the Type I crystal lattice are shown beside a cartoon of phospholipid bilayers (right). The pore module (PM) and voltage-sensor domains (VSD) are indicated. The VSDs appear to be particularly devoid of lattice distortions: the extracellular loops are completely free from direct crystal contacts (1, green circle) and only a minor contact is observed between the S1N helix and the intracellular S2-S3 loop (2, green circle). **b,** Six (of seven) phospholipids per subunit seen bound to NavAb are shown on one side of the channel. OL and IL represent the outer and inner leaflets of the membrane bilayer, respectively. Electron-densities are from F_o-F_c omit maps (NavAb-Ile217Cys, 2.8 Å structure) contoured at 2.5 σ. **c,** NavAb channels colored according to crystallographic temperature factors of the main-chain (blue < 50 Å^2 to red > 150 Å^2). These values are within the expected range for the diffraction characteristics of the NavAb crystals (see Methods).

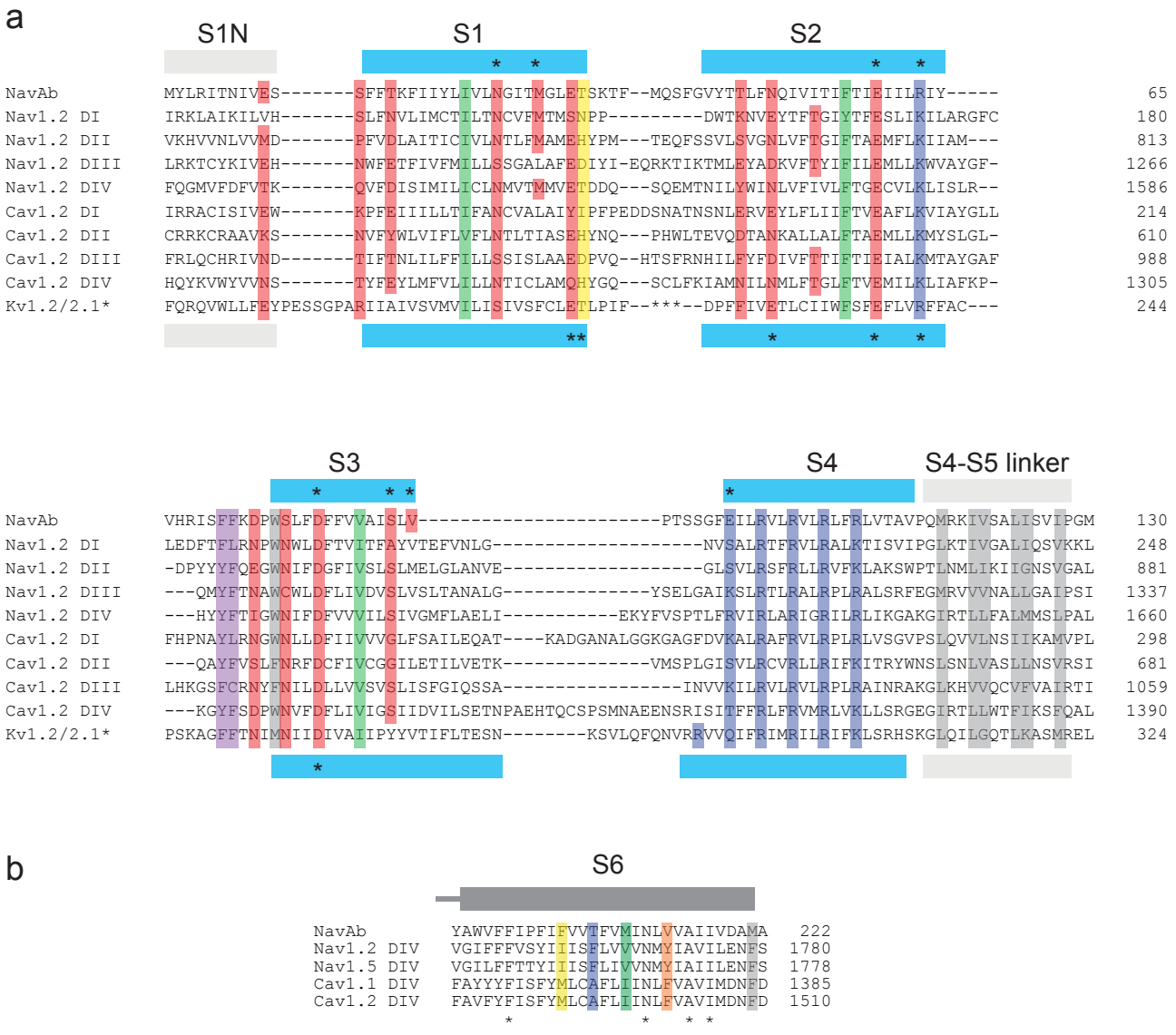

Supplementary Figure 7. Structure-based sequence alignment of multiple VSDs. a, High-resolution crystal structures are now available for NavAb (top sequence) and the K_V1.2/2.1 channel (bottom sequence, PDB - 2R9R; note that the large insertion in the S1-S2 loop of K_V1.2/2.1 has been removed for clarity). These sequences are aligned against Domains I through IV of the well-studied Na_V1.2 (rat) and the Ca_V1.2 (rabbit) channels. Residues discussed in the main text are highlighted here. Intracellular (INC) and extracellular (ENC) negative charge-cluster residues and other (partially) conserved polar positions within the VSD are shown in orange, and the three conserved hydrophobic constriction site (HCS) residues are highlighted in green. The "conserved" S1 threonine residue that may interact with the P-helix is shown in yellow; partial conservation at this position suggests the possibility that a similar VSD-P-helix hydrogen bonding interaction may be available within the VSDs of other VGICs[15], but may be mediated through a side-chain other than threonine. The amphipathic nature and conserved length of the S4-S5 linker is also indicated. Also note the high conservation of the positively charged residue at the intracellular end of S2 (Arg63 in NavAb), which in both NavAb (Fig. 1e) and K_V1.2/2.1 structures[16], interacts with residues from the intracellular negative charge-cluster. Polar residues within the VSD that interact with gating charges (or the P-helix) in NavAb and K_V1.2/2.1 crystal structures have been indicated by an *. **b,** Sequence alignment of the S6 pore-lining segments from NavAb, Na_V1.2, Na_V1.5, Ca_V1.1 and Ca_V1.2. Phe203 of NavAb (yellow) forms the main "gate" over the pore fenestration (Fig. 4a, b). Other residues implicated in drug binding and block in Na_V and Ca_V channels are highlighted (blue, green and orange). Met221 in NavAb (grey) seals the intracellular gate (Supplementary Fig. 4c).

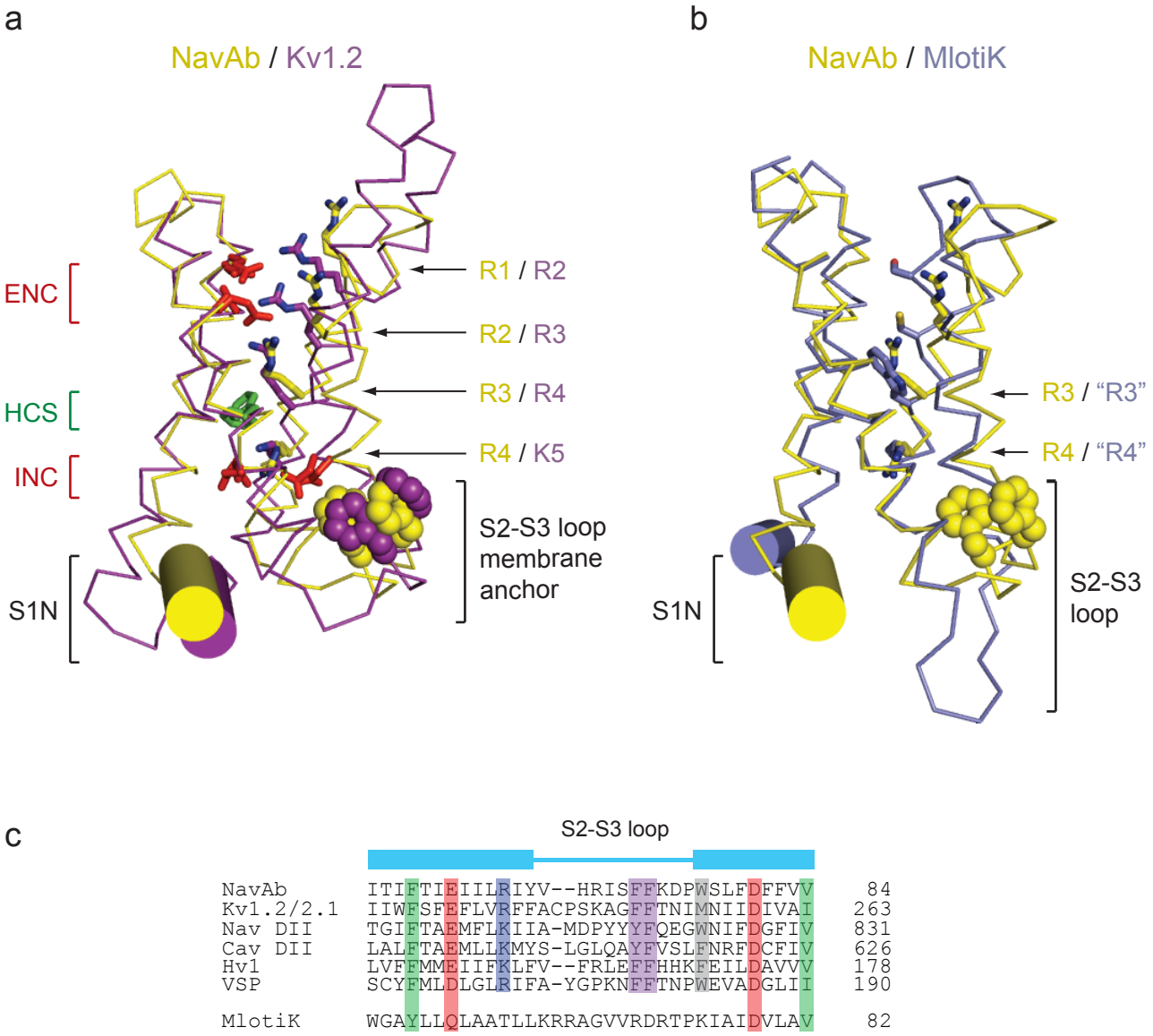

Supplementary Figure 8. Structural superposition of the NavAb, K_V1.2/2.1 and MlotiK VSDs. **a,** Superposition of NavAb (yellow) and K_V1.2/2.1 (purple; PDB - 2R9R) VSDs demonstrates their structural likeness. Residues from the extracellular and intracellular negative charge-clusters (ENC and INC) are colored red, the conserved phenylalanine residues lining the hydrophobic constriction site (HCS) of the gating pore are colored green, and the conserved phenylalanine resides within the S2-S3 loop are shown as sphere representations. Positionally-equivalent S4 gating charges and the S1N helices have also been indicated. Notice that the S4 segments are in similar and activated conformations. **b,** Superposition of the VSDs from NavAb (yellow) and the non-voltage gated K^+-channel MlotiK (blue; PDB - 3BEH) suggest that their S4 segments are in comparable conformations. Here, we wish to highlight the lack of correspondence between the S1N helices and S2-S3 loops of NavAb and MlotiK. In MlotiK, the S1N helix points in the opposite direction and the S2-S3 loop appears to be "soluble" (also see part **c**). **c,** Structure-based sequence alignment between evolutionarily distant VSDs demonstrates the conservation of functional and structural residues across the VGIC family within the S2-S3 loop region. All sequences shown are from members of the VGIC superfamily: NavAb, K_V1.2/2.1, rat Na_V1.2 (domain II), rabbit Ca_V1.2 (domain II), the human voltage-gated proton channel (Hv1), and the Ciona voltage-activated phosphatase (VSP). Trp76 in NavAb (grey) demarks the beginning of the S3 segment. Conserved residues of the hydrophobic constriction site (green; HCS), intracellular negative charge-cluster (orange; INC), phenylalanine/aromatic residues in the S2-S3 loop (purple), and basic S2 residue (blue; Arg63 in NavAb).

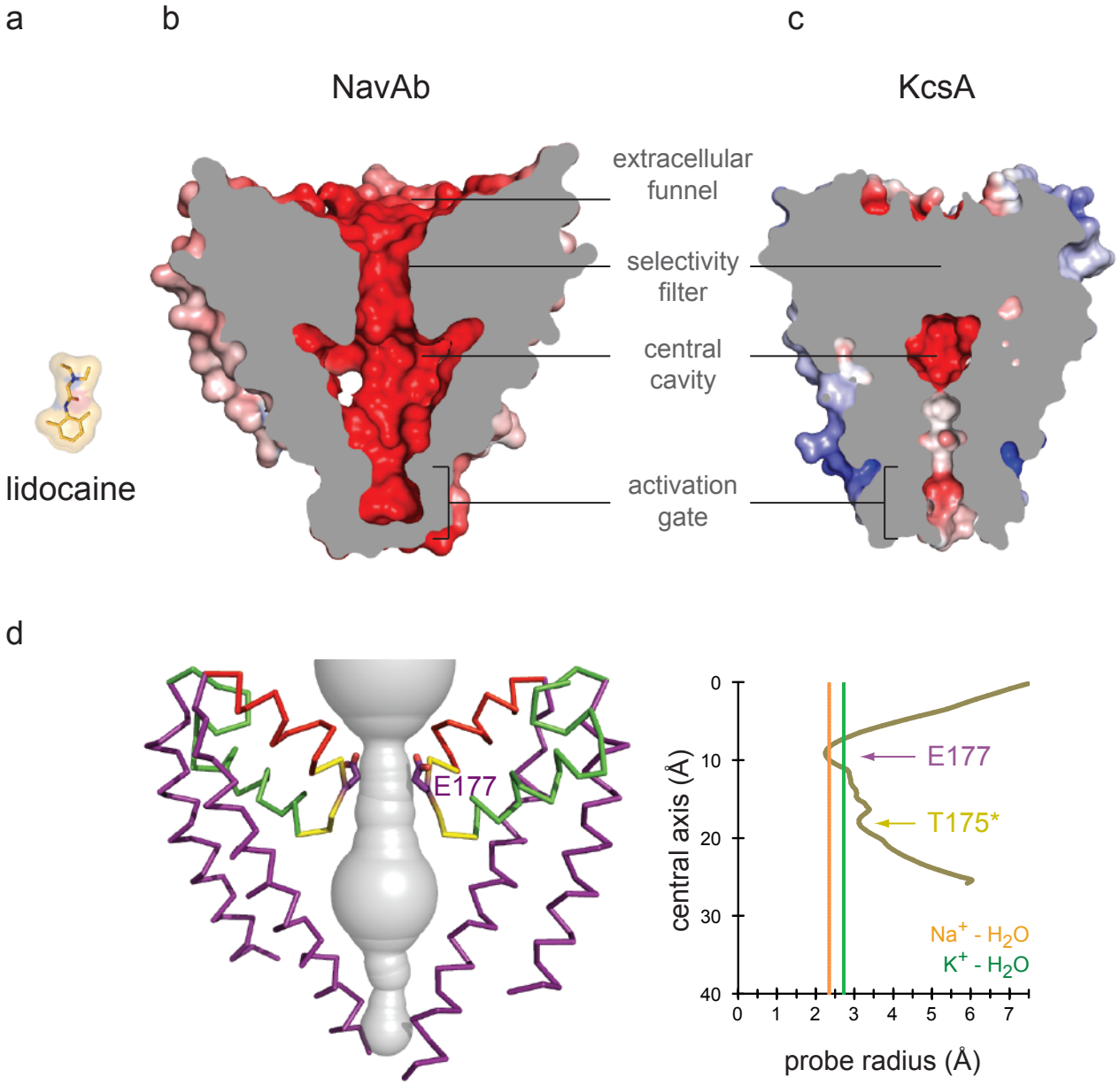

Supplementary Figure 9. Comparison of NavAb and K^+-selective channel pores. a, A stick and surface representation of lidocaine, a typical Na_V channel blocking drug, is shown to scale for illustrative purposes. **b-c,** Electrostatic surfaces of NavAb and a closed K^+-selective channel (KcsA, PDB - 1K4C) were calculated using the APBS software[17] with 150 mM NaCl in the solvent (colored from -10 to 10 kT, red to blue). The unique surface and electrostatic features of the extracellular funnel, the selectivity filter, and the central cavity of NavAb can be appreciated here. It is likely that these features have consequences for the mechanism of ion conduction in NavAb, as well as for ion and/or drug binding and block in Na_V and Ca_V channels. Due to its narrowness, the K^+-channel selectivity filter is obscured in this representation. **d,** Pore radius of NavAb. Glu177 side-chains are shown as purple stick representations. A probe of the van der Waals pore radius is shown (grey) and compared (within the selectivity filter region) to the radii of a Na^+-H_2O complex (orange) and a K^+-H_2O complex (green). Pore chemistry and hydrogen bonding potential are not considered here. Thr175* denotes the backbone carbonyl of Thr175.

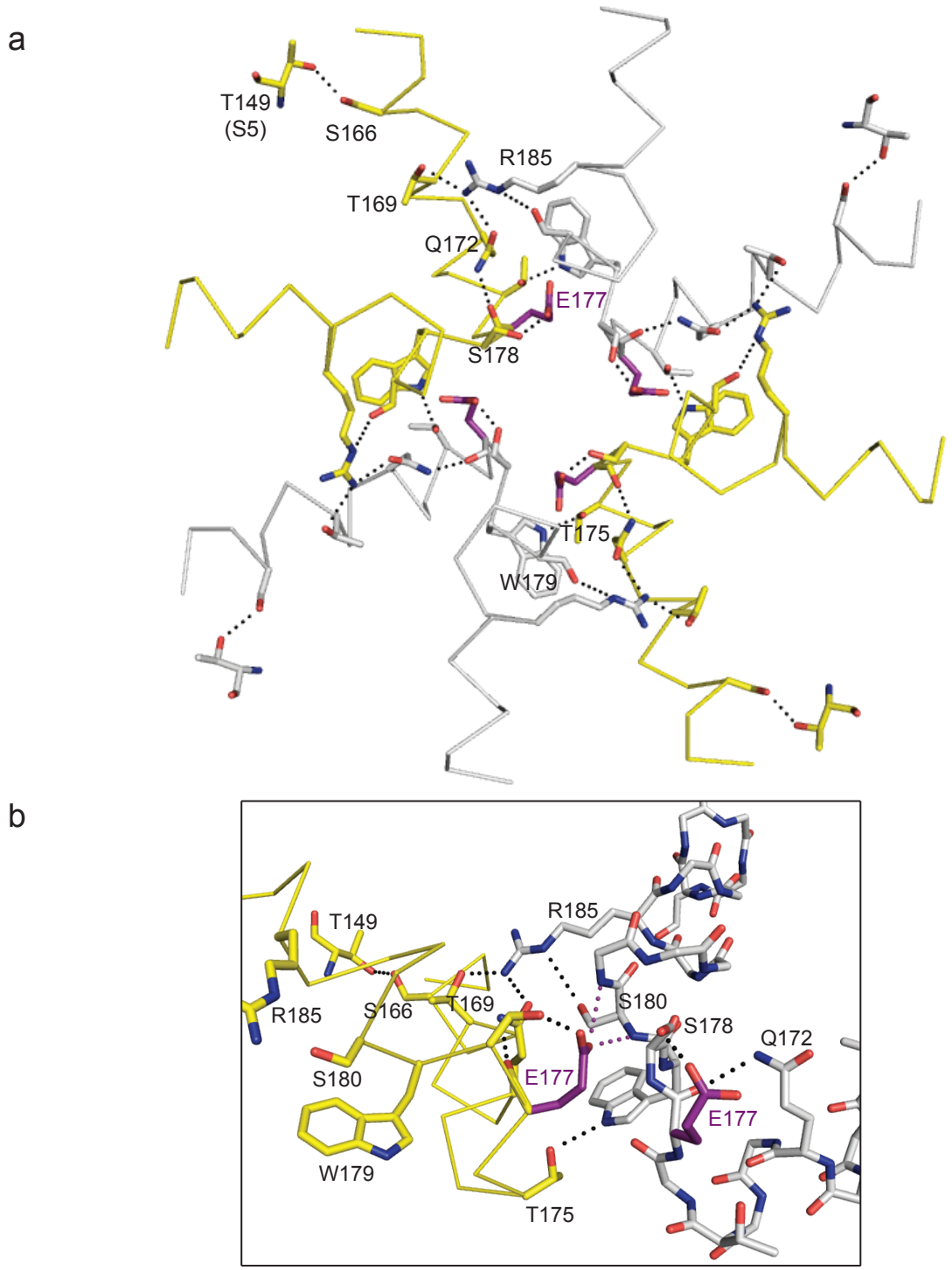

Supplementary Figure 10. Conserved interaction network within the NavAb pore module. **a,** Interactions within the NavAb pore module are viewed from the extracellular side of the membrane. Dashed-lines indicate all potential hydrogen bond interactions observed between highly conserved pore residues in NavAb, as assessed from the multi-sequence alignment of the bacterial Na_V channels shown in Supplementary Fig. 1. An interconnected-network of interactions is centered around the selectivity filter-lining Glu177 residues, but these interactions also extend throughout the P- and P2-helices. For example, a highly-conserved P-helix-S5 hydrogen bonding interaction is illustrated (Ser166-Thr149). Overall, this interaction network likely has a role in determining the structure and stability of the pore and selectivity filter in NavAb. **b,** Expanded from part **a** with a different view. The Glu177 side-chain interactions with the backbone amides of Ser180 and Met181 from the P2-helix of a neighboring subunit have been highlighted in purple.

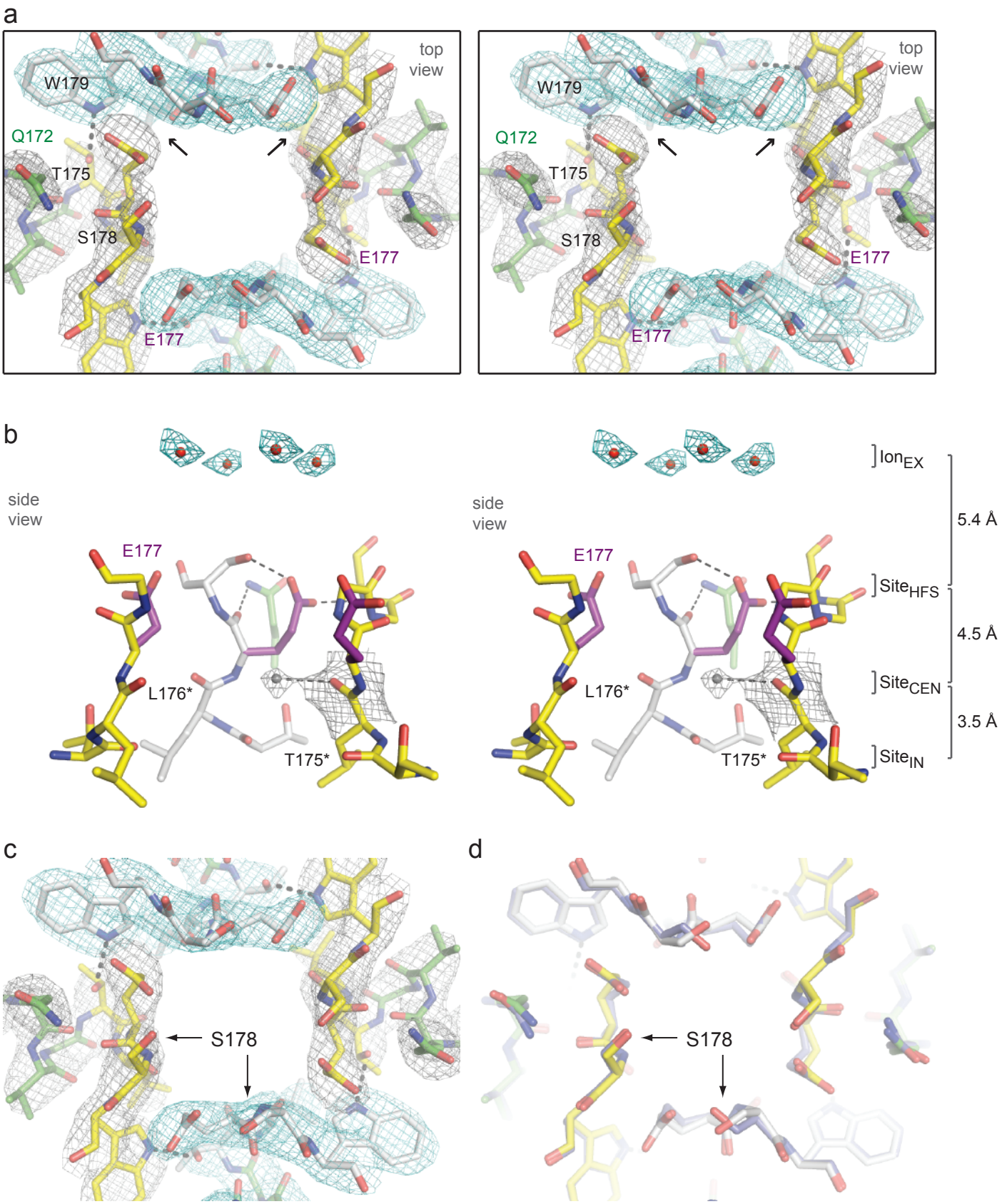

Supplementary Figure 11. Structure of the NavAb selectivity filter.
See Figure legend on next page.

Supplementary Figure 11. Structure of the NavAb selectivity filter. a, Top-view of the NavAb-Ile217Cys selectivity filter in stereoview. Symmetry-related molecules are colored white and yellow, respectively, and P-helix residues are green. The hydrogen bond between Thr175 and Trp179 is indicated by a dashed line (grey). Electron-density maps are from F_o-F_c omit maps contoured at 4.0 σ (blue and grey) and subtle difference can be appreciated (small arrows). **b,** Side-view of the NavAb-Ile217Cys selectivity filter in stereoview. Glu177 (purple) interactions with Gln172, Ser178 and the backbone of Ser180 (Ser180 from the neighboring subunit) are shown in the far subunit. An F_o-F_c omit map contoured at 4.75 σ (blue) and putative cations or water molecules (red spheres, Ion_{EX}) are shown. Electron density around Leu176 (grey, F_o-F_c contoured at 1.75 σ) and a putative water molecule is also shown (grey sphere). **c,** Top-view of the NavAb-Met221Cys selectivity filter in standard view. Colored as in part **a**. Electron-density maps are from F_o-F_c omit maps contoured at 3.5 σ (blue and grey), which defines different orientations for the Ser178 side-chains between the crystallographically independent subunits. **d,** Superposition between the NavAb-Ile217Cys structure (blue) and NavAb-Met221Cys structure (colored as in part **c**) indicates their overall structural similarity. Only the orientation of two Ser178 side-chains (of the four) is markedly different. This suggests that the nearby Glu177 side-chains can experience different structural (and chemical) environments. We note that the Ser178 side-chain does not appear to play an essential role in Na^+ selectivity in NaChBac[7].

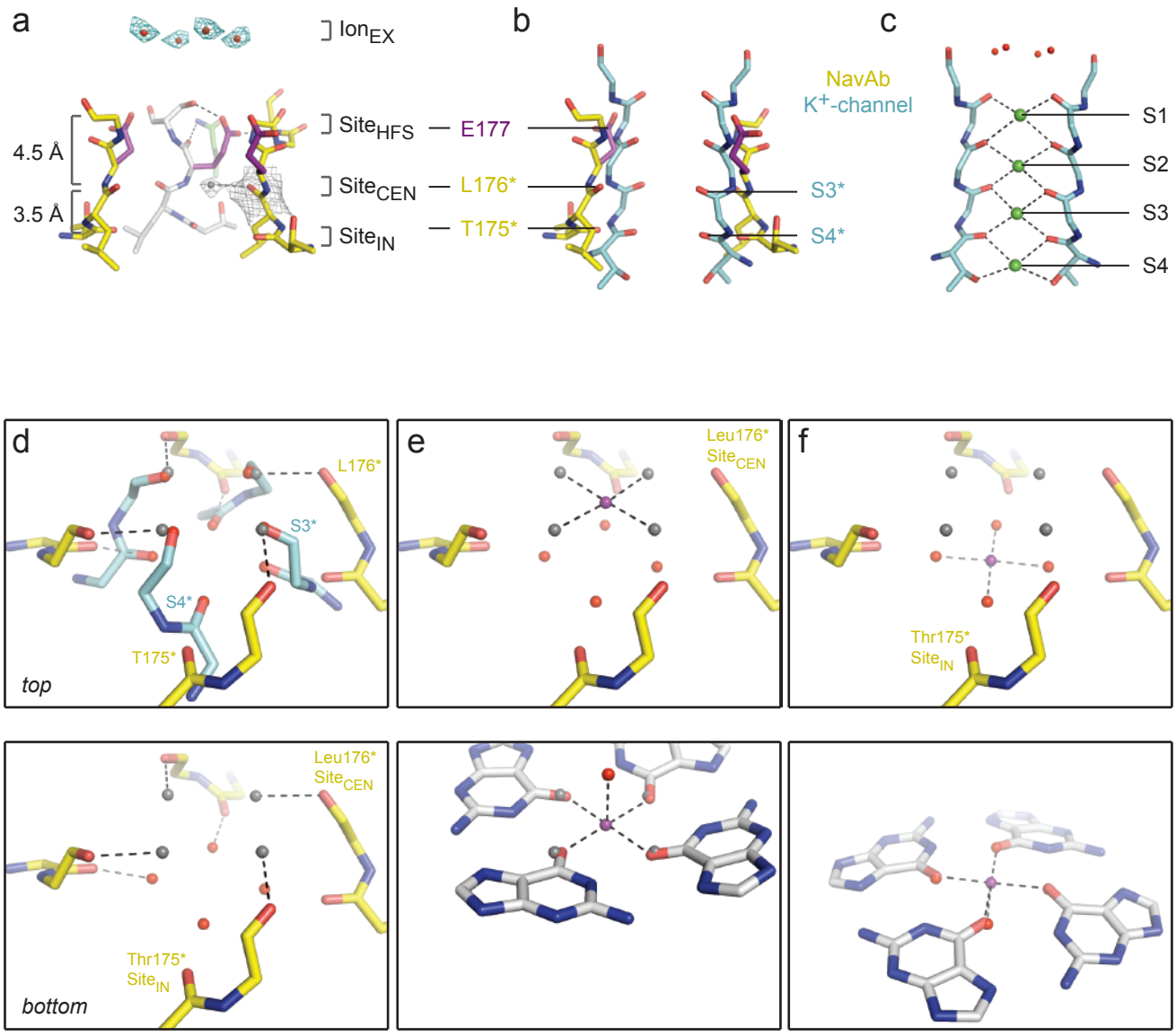

Supplementary Figure 12. Modeling of potential ion interaction sites within the NavAb selectivity filter. See figure legend on next page.

Supplementary Figure 12. Modeling of potential ion interaction sites within the NavAb selectivity filter. a, Side-view of the NavAb selectivity filter reproduced from Fig. 3b, where electron-density above the selectivity filter (blue) and for putative water molecules off the Leu176 carbonyl (grey) have already been described. The distance from the Leu176 carbonyl ($Site_{CEN}$) to the modeled water molecule is 2.5 Å and is consistent with a strong hydrogen bond. **b,** Superposition of NavAb and a K^+-channel selectivity filter was performed based only on their P-helices (PDB - 1K4C). The backbone carbonyls (*) of Leu176 and Thr175 from NavAb and the "site 3" and "site 4" carbonyls from the K^+-channel have been indicated. Only two subunits have been shown for clarity (yellow, NavAb; cyan, K^+-channel). **c,** Structure of a K^+-channel selectivity filter with four low-energy K^+ binding sites occupied by K^+ ions (green spheres) is shown for comparative purposes (PDB - 3LDC; waters above the filter are shown as red spheres). Details of the proposed conduction mechanism have been described elsewhere, but the four binding sites are expected to be occupied by K^+ ions in either a site 1,3 or site 2,4 configuration with intervening water molecules[18,19]. Only two subunits have been shown here for clarity. **d, *Top.*** An expanded view from part **b** with selectivity filter ligands from all four channel subunits shown and the four putative water molecules modeled into the NavAb electron density maps represented as grey spheres. The four putative water molecules (grey spheres) are 2.5 Å off the backbone carbonyls of Leu176 and superimpose onto the site 3 carbonyls from the K^+-channel selectivity filter. The two distances indicated between the Thr175 carbonyls of NavAb and the site 4 carbonyls from the K^+-channel both measure 2.5 Å, and this geometry approximates an ideal coordination scheme for (hypothetical) water molecules that may be bound off the Thr175 backbone carbonyls of NavAb. ***Bottom.*** Same view as above with the K^+-channel removed for clarity, but with the K^+-channel site 4 carbonyl oxygen atoms left behind to represent hypothetical water molecules (red spheres). The distance from the Thr175 carbonyls to the hypothetical water molecules (red spheres) is 2.5 Å, indicative of a strong hydrogen bond. In addition to the modeling shown in parts **e-f**, these candidate water molecule locations could also represent the potential sites for hydrated Na^+ ions to be coordinated directly onto the carbonyls of Leu176 and Thr175. **e,** A proposed Na^+ ion coordination scheme at $Site_{CEN}$ in NavAb. ***Top.*** Numerous experimental structures and computational studies suggest that Na^+ ions tend to coordinate four oxygen atoms (either from carbonyls or water molecules, for example) "in plane" to assume a square pyramidal or square bipyramidal coordination scheme[19-28]. The four planar waters off Leu176 (grey spheres) are shown coordinating a centrally located (hypothetical) Na^+ ion. ***Bottom.*** A square pyramidal Na^+ coordination site from a 0.95 Å resolution crystal structure of a guanine tetraplex[20] that displays ideal Na^+-coordination geometry is superimposed onto the putative Leu176 water molecules of NavAb (grey spheres). The excellent superposition of the O6 oxygen atoms with the Leu176 water molecules demonstrates the chemical basis for the Na^+-coordination scheme proposed in the ***Top*** panel. **f,** A proposed Na^+ ion coordination scheme at $Site_{IN}$ in NavAb. See part **e** for a detailed description.

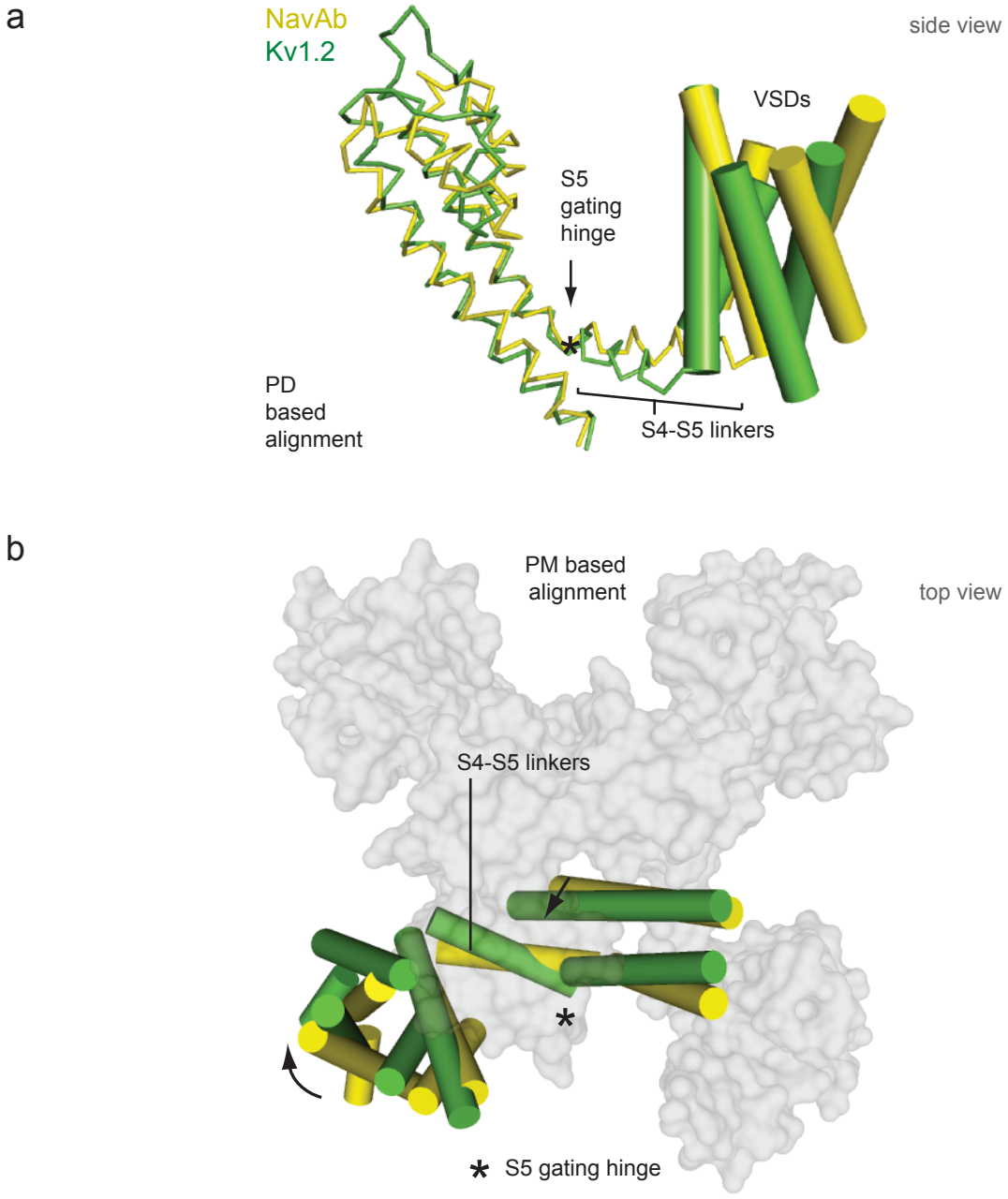

Supplementary Figure 13. Components and model of activation gate opening in VGICs. **a,** Superposition of NavAb (yellow) and K_V1.2/2.1 (green, 2R9R) subunits based only on their pore domains (shown as backbone Cα ribbons). The overall likeness between the closed (NavAb) and open (K_V1.2/2.1) pore domain subunit structures suggests a tight structural-coupling between the S5-S6 helices in VGICs. **b,** Superposition of the entire NavAb and K_V1.2/2.1 tetrameric pore modules (PM) based on their P-helices, one complete subunit is shown as cylinders. The view is from the extracellular side. Two rigid-body motions can be seen around the S5 gating hinge: one for the PMs (S5-S6) and one for the S4-S5 linkers/VSDs. The spatial relationship among the α-helices within each of these two bundles remains relatively constant as the VSD rolls over the PM, pivoting at the base of the S5 segment. Based on steric considerations, pore opening will be concerted when the S5-S6 segments move from the closed pore (yellow) to open pore (green). The S4-S5 linker pivots along the membrane interface (also see Fig. 5b) and the largest displacements occur at the intracellular side of the VSD (e.g. the S1N helix).

Supplemental References

1 Pavlov, E. *et al.* The pore, not cytoplasmic domains, underlies inactivation in a prokaryotic sodium channel. *Biophys J* **89**, 232-242 (2005).

2 Benitah, J. P., Chen, Z., Balser, J. R., Tomaselli, G. F. & Marban, E. Molecular dynamics of the sodium channel pore vary with gating: interactions between P-segment motions and inactivation. *J Neurosci* **19**, 1577-1585 (1999).

3 Hilber, K. *et al.* Selectivity filter residues contribute unequally to pore stabilization in voltage-gated sodium channels. *Biochemistry* **44**, 13874-13882 (2005).

4 Todt, H., Dudley, S. C., Jr., Kyle, J. W., French, R. J. & Fozzard, H. A. Ultra-slow inactivation in mu1 Na^+ channels is produced by a structural rearrangement of the outer vestibule. *Biophys J* **76**, 1335-1345 (1999).

5 Xiong, W. *et al.* A conserved ring of charge in mammalian Na^+ channels: a molecular regulator of the outer pore conformation during slow inactivation. *J Physiol* **576**, 739-754 (2006).

6 Cuello, L. G., Jogini, V., Cortes, D. M. & Perozo, E. Structural mechanism of C-type inactivation in K^+ channels. *Nature* **466**, 203-208 (2010).

7 Yue, L., Navarro, B., Ren, D., Ramos, A. & Clapham, D. E. The cation selectivity filter of the bacterial sodium channel, NaChBac. *J Gen Physiol* **120**, 845-853 (2002).

8 Ren, D. *et al.* A prokaryotic voltage-gated sodium channel. *Science* **294**, 2372-2375 (2001).

9 Koishi, R. *et al.* A superfamily of voltage-gated sodium channels in bacteria. *J Biol Chem* **279**, 9532-9538 (2004).

10 Ito, M. *et al.* The voltage-gated Na^+ channel Na_VBP has a role in motility, chemotaxis, and pH homeostasis of an alkaliphilic *Bacillus*. *Proc Natl Acad Sci U S A* **101**, 10566-10571 (2004).

11 Irie, K. *et al.* Comparative study of the gating motif and C-type inactivation in prokaryotic voltage-gated sodium channels. *J Biol Chem* **285**, 3685-3694 (2010).

12 Mio, K., Mio, M., Arisaka, F., Sato, M. & Sato, C. The C-terminal coiled-coil of the bacterial voltage-gated sodium channel NaChBac is not essential for tetramer formation, but stabilizes subunit-to-subunit interactions. *Prog Biophys Mol Biol* **103**, 111-121 (2010).

13 Powl, A. M., O'Reilly, A. O., Miles, A. J. & Wallace, B. A. Synchrotron radiation circular dichroism spectroscopy-defined structure of the C-terminal domain of NaChBac and its role in channel assembly. *Proc Natl Acad Sci U S A* **107**, 14064-14069 (2010).

14 Terwilliger, T. *SOLVE and RESOLVE: Automated Structure Solution and Density Modification.*, Vol. 374 22-37 (Elsevier, 2003).

15 Lee, S. Y., Banerjee, A. & MacKinnon, R. Two separate interfaces between the voltage sensor and pore are required for the function of voltage-dependent K^+ channels. *PLoS Biol* **7**, e47 (2009).

16 Long, S. B., Tao, X., Campbell, E. B. & MacKinnon, R. Atomic structure of a voltage-dependent K^+ channel in a lipid membrane-like environment. *Nature* **450**, 376-382 (2007).

17 Baker, N. A., Sept, D., Joseph, S., Holst, M. J. & McCammon, J. A. Electrostatics of nanosystems: application to microtubules and the ribosome. *Proc Natl Acad Sci U S A* **98**, 10037-10041 (2001).

18 Morais-Cabral, J. H., Zhou, Y. & MacKinnon, R. Energetic optimization of ion conduction rate by the K^+ selectivity filter. *Nature* **414**, 37-42 (2001).
19 Ye, S., Li, Y. & Jiang, Y. Novel insights into K^+ selectivity from high-resolution structures of an open K^+ channel pore. *Nat Struct Mol Biol* **17**, 1019-1023 (2010).
20 Phillips, K., Dauter, Z., Murchie, A. I., Lilley, D. M. & Luisi, B. The crystal structure of a parallel-stranded guanine tetraplex at 0.95 Å resolution. *J Mol Biol* **273**, 171-182 (1997).
21 Thompson, A. N. *et al.* Mechanism of potassium-channel selectivity revealed by Na^+ and Li^+ binding sites within the KcsA pore. *Nat Struct Mol Biol* **16**, 1317-1324 (2009).
22 Alam, A. & Jiang, Y. Structural analysis of ion selectivity in the NaK channel. *Nat Struct Mol Biol* **16**, 35-41 (2009).
23 Harding, M. M. Metal-ligand geometry relevant to proteins and in proteins: sodium and potassium. *Acta Crystallogr D Biol Crystallogr* **58**, 872-874 (2002).
24 Noskov, S. Y. & Roux, B. Importance of hydration and dynamics on the selectivity of the KcsA and NaK channels. *J Gen Physiol* **129**, 135-143 (2007).
25 Bucher, D., Guidoni, L., Carloni, P. & Rothlisberger, U. Coordination numbers of K^+ and Na^+ Ions inside the selectivity filter of the KcsA potassium channel: insights from first principles molecular dynamics. *Biophys J* **98**, L47-49 (2010).
26 Shrivastava, I. H., Tieleman, D. P., Biggin, P. C. & Sansom, M. S. K^+ versus Na^+ ions in a K channel selectivity filter: a simulation study. *Biophys J* **83**, 633-645 (2002).
27 Doi, M. *et al.* Caged and clustered structures of endothelin inhibitor BQ123, cyclo(-D-Trp-D-Asp--Pro-D-Val-Leu-)-Na^+, forming five and six coordination bonds between sodium ions and peptides. *Acta Crystallogr D Biol Crystallogr* **57**, 628-634 (2001).
28 Derebe, M. G., Zeng, W., Li, Y., Alam, A. & Jiang, Y. Structural studies of ion permeation and Ca^{2+} blockage of a bacterial channel mimicking the cyclic nucleotide-gated channel pore. *Proc Natl Acad Sci U S A* **108**, 592-597 (2010).